*sustainability*

MDPI

*Article*

# One-Step Electrosynthesis of Bifunctional NiCu Nanosheets on Iron Foam for Remarkably Enhanced Alkaline Water Splitting

**Zhenwei Liu [1], Qiang Wang [2], Qingxiang Kong [1,3], Xiaoning Tong [1], Song Wu [1], Naixuan Zong [1,3], Ruidong Xu [1,3,*] and Linjing Yang [1,*]**

[1] Faculty of Metallurgical and Energy Engineering, Kunming University of Science and Technology, Kunming 650093, China; 20212102025@stu.kust.edu.cn (Z.L.); 20212228012@stu.kust.edu.cn (Q.K.); 20212102050@stu.kust.edu.cn (X.T.); 20212102022@stu.kust.edu.cn (S.W.); 20212228021@stu.kust.edu.cn (N.Z.)
[2] 2020 X-Lab, Shanghai Institute of Microsystem and Information Technology, Chinese Academy of Sciences, Shanghai 200050, China; wangqiang@mail.sim.ac.cn
[3] State Key Laboratory of Complex Nonferrous Metal Resources Clean Utilization, Kunming University of Science and Technology, Kunming 650093, China
* Correspondence: rdxupaper@aliyun.com (R.X.); eslinjingyang@kust.edu.cn (L.Y.); Tel.: +86-871-65160072 (R.X.); +86-871-65160072 (L.Y.)

**Abstract:** Electrocatalytic water splitting for hydrogen production driven by renewable electricity offers a promising way of achieving energy sustainability, but the design of highly efficient and cost-effective electrocatalysts is regarded as a bottleneck. Herein, a bifunctional microflowers NiCu is successfully deposited on an iron foam (IF) electrode via one-step electrolysis of spend cupronickel (SCN). Unexpectedly, the designed IF-supported NiCu (NiCu/IF) electrocatalysts exhibit excellent catalytic performance for oxygen evolution reactions (OER) and hydrogen evolution reactions (HER) in 1 M KOH. Only 98 and 267 mV are required to drive a current density of 10 mA $cm^{-2}$ for HER and OER, respectively. Importantly, the self-supported NiCu/IF electrode requires a low cell voltage of 1.57 V to achieve 10 mA $cm^{-2}$ of alkaline overall water splitting with extremely high stability. With the introduction of a glycerol oxidation reaction (GOR), the HER performance is further remarkably enhanced with an extremely low cell voltage of 1.29 V at 10 mA $cem^{-2}$, highlighting an attractive energy-efficient hydrogen production coupled with biomass conversion process. This study reports a novel synthesis strategy for low-cost and high-performance Ni-based nanostructure catalysts using SCN as precursors, which is of vital significance for green hydrogen production and waste recycling.

**Keywords:** bifunctional electrocatalysts; water splitting; spend cupronickel; soluble anode; electrosynthesis



**Citation:** Liu, Z.; Wang, Q.; Kong, Q.; Tong, X.; Wu, S.; Zong, N.; Xu, R.; Yang, L. One-Step Electrosynthesis of Bifunctional NiCu Nanosheets on Iron Foam for Remarkably Enhanced Alkaline Water Splitting. *Sustainability* **2023**, *15*, 12240. https://doi.org/10.3390/su151612240

Academic Editor: Md. Shahinoor Islam

Received: 25 June 2023
Revised: 3 August 2023
Accepted: 9 August 2023
Published: 10 August 2023



## 1. Introduction

Water electrolysis for hydrogen production can store renewable clean energy (e.g., solar energy), and is thus regarded as the most desirable strategy for settling the deteriorating environmental pollution and energy scarcity problems [1–5]. The water electrolysis process consists of two half-reactions: the cathodic hydrogen evolution reaction (HER) and the anodic oxygen evolution reaction (OER) [6]. They generally demand high overpotentials owing to the sluggish kinetics and complex electron transfer process to drive the thermodynamically uphill reaction [7,8]. Presently, the benchmark Pt-based catalysts for HER and Ru/Ir oxides for OER are in the commercialization process of hydrogen production by water splitting [8]. However, these noble metal electrocatalysts have been greatly limiting the development of water electrolysis technology due to their scarcity and high cost [9]. Thus, the design of low-cost, high-performance electrocatalysts based on earth-abundant elements to replace precious metals is highly desired [10]. Alternatively, using a bifunctional electrocatalyst to simultaneously reduce the overpotentials of HER and OER is an effective way to achieve highly efficient overall water splitting [11,12].

Recently, numerous cost-effective transition-metal-based electrocatalysts have been reported for water splitting, such as phosphides [13,14], nitride [15,16], oxides [17,18], hydroxides [19,20], carbides [21,22] and alloys [23–25]. Among them, nickel-based nanomaterials are considered one of the most promising HER catalysts due to the fact that they are plentiful and cheap, as well as their outstanding corrosion resistance in alkaline environments and Pt-like HER properties. Yan Shulei et al. studied the hydrogen adsorption energy ($\Delta G_H$) of Ni-based bimetallic and found that the M-H synergy bonds can optimize the d-band center of the alloy. Among them, the ΔGH of NiCu is close to zero. Adopting simple electrochemical oxidation to introduce oxygen atoms to balance the adsorption/desorption process of the catalyst for OH* greatly improved HER activity of O-NiCu [26]. Moreover, the active intermediate NiOOH formed during the water oxidation process has a superior electrocatalytic activity for OER thorough reducing the reaction energy barrier and accelerating the kinetic process. Specifically, Subbaraman et al. synthesized transition-metal (Mn, Fe, Co, and Ni) hydr(oxy)oxides and found their OER activity followed the order Ni, Co, Fe, and Mn [27]. Similarly, Dai et al. prepared Ni/$Ni(OH)_2$ nanosheets with low overpotentials of 77 and 270 mV at 10 mA $cm^{-2}$ for the HER and OER, respectively [28]. Therefore, as the best choice, nickel-based catalysts are ideal bifunctional electrocatalysts with the advantages of low cost and environmental friendliness [29].

In addition, biomass and its derivatives (such as methanol, ethanol, glycerol, sugars, etc.) are regarded as renewable hydrogen resources since they contain a lot of hydrogen. Moreover, it was found that these biomass molecules can not only greatly accelerate the cathodic HER, but also produce various high added-value products [30]. Hence, replacing the sluggish and low-added OER with thermodynamically more favorable anodic reactions (i.e., biomass oxidation) has been extensively demonstrated to effectively accelerate hydrogen generation and simultaneously stabilize the electrocatalysts [31,32]. For example, glycerol-assisted hybrid water electrolysis has recently attracted increasing attention because the glycerol oxidation reaction (GOR) can not only achieve energy-efficient hydrogen production but also produce high-value chemicals such as formate at the anode [33–42].

Although great achievements have been acquired in the fabrication of efficient, low-cost transition metal bifunctional electrocatalysts [43] An unavoidable issue is that the transition metal resource is not infinite and thus not ideal for the long term, and further reducing the cost of electrocatalysts is conducive to the development of hydrogen energy. Consequently, the transformation from secondary metal resources into efficient electrocatalysts is a meaningful way to supersede the conventional stereotype of catalyst synthesis based on the finished reagents. As an indispensable alloy material, cupronickel has been widely used in various fields such as precise instruments, medical equipments, automotive parts, elastic components, and daily necessities because of its excellent mechanical properties [44,45]. Furthermore, the output of cupronickel waste is increasing along with the rapid development of modern industrialization [44]. Therefore, the sustainable and efficient recycling of valuable metal resources (e.g., Ni and Cu) is very significant. Presently, it is difficult to achieve the efficient separation of copper, nickel and other non-ferrous metals in the traditional pyrometallurgical process and the high cost and pollutant emission can hardly be avoided in the hydrometallurgy process. It is thus obvious that it is far-reaching research to produce superior catalytic activity bifunctional catalysts with simple and easy-to-operate routes. In this context, electrolytic synthesis has emerged as an attractive technology for the fabrication of transition metal electrocatalysts due to its simple, controllable, and energy-efficient process [46,47].

Herein, we provide present a simple one-step electrosynthesis approach to fabricate efficient spend cupronickel (SCN) and robust bifunctional NiCu electrocatalysts using the SCN as a soluble anode. The NiCu microflowers, which are composed of nanometer-thick flakes tightly deposited on the porous iron foam (IF), show excellent electrocatalytic performance for alkaline overall water splitting. Moreover, such an integrated NiCu/IF electrode also exhibits enhanced HER due to the replacement of OER by GOR. Our work may open a

new avenue for developing high-performance transition-metal-based electrocatalysts with microflowers for hydrogen production and biomass upgrading.

## 2. Materials and Methods

### *2.1. Reagents and Chemicals*

SCN alloy was purchased from Dongguan Yang Chong metal material Co., Ltd. (Dongguan, China), which mainly contains copper, nickel, zinc and other elements (Table S3). A total of 98 wt% concentrated $H_2SO_4$ and 38 wt% concentrated HCl were obtained from Chongqing Chuandong Chemical (Group) Co., Ltd. (Nanan, China) and Sichuan Xilong Science Co., Ltd. (Chengdu, China), respectively. The IF was bought from Kunshan Guangjiayuan New Material Co., Ltd. (Kunshan, China). Anhydrous ethanol was acquired from Chengdu Chron Chemicals Co., Ltd. (Chengdu, China).

### *2.2. Material Synthesis*

#### 2.2.1. Preparation of NiCu/IF and CN/IF Electrodes

Before the electrosynthesis process, the SCN ($40 \times 40 \times 3$ mm$^3$) and porous IF ($20 \times 20 \times 1$ mm$^3$) substrates were subjected to a series of pre-treatments, including mechanical polishing, ultrasonication in 3 M HCl solution, and rinsing with deionized (DI) water and acetone, followed by vacuum drying at 60 °C. As for the preparation of NiCu/IF electrode, a simple electrolysis method was employed using SCN and IF as anode and cathode, respectively, in 0.1 M $NiSO_4$ solution at 60 °C. During the electrolysis process, a current density of 37.5 mA cm$^{-2}$ was kept for 10 min. As a referential sample, the CN/IF electrode was also prepared in 0.1 M $H_2SO_4$ solution using the above-mentioned processes.

#### 2.2.2. Fabrication of IF-Supported Pt/C and $RuO_2$

To prepare the $RuO_2$ and 20 wt% Pt/C electrodes, 40 mg active material (either iridium oxide or Pt on carbon) was uniformly dispersed in a mixture solution containing 90 μL Nafion solution, 810 μL ethanol, and 600 μL DI water with the assistance of vigorous stirring and sonication. A piece of cleaned IF electrode was then soaked in the solution for 1 h to let the active material coat the surface, followed by drying in air [48].

### *2.3. Chemical and Structural Characterization*

The phase compositions, chemical constitution, surface microstructure, element composition and chemical state of the synthetic composite electrode NiCu/IF were surveyed using X-ray diffraction (XRD, D/Max 2200, Rigaku Co, Tokyo, Japan) technology, Thermo Fischer DXR, field emission scanning electron microscopy (FE-SEM, Nova Nano SEM 450, Thermo Fisher Scientific, New York, NY, USA), and X-ray photoelectron spectroscopy (XPS, PHI 5500, Nihon Philips Corp, Tokyo, Japan). Transmission Electron Microscope (TEM) measurements were executed by the JEM-2100 instrument. Raman spectroscopy (Thermo Fischer DXR, Thermo Fisher Scientific) was used to observe the material changes of the samples. The elemental content of the NiCu/IF electrode and SCN were investigated using inductively coupled plasma-mass spectrometry (ICP, Agilent 5110(OES), Agilent Technologies Inc., New York, NY, USA).

### *2.4. Electrochemical Measurements*

The electrochemical measurements were performed using CHI 760E electrochemical station using a standard three-electrode system where a graphite rod, Ag/AgCl electrode, and the as-prepared electrocatalyst were used as the counter electrode, reference electrode, and working electrode, respectively. A 1 M KOH aqueous solution (pH = 14) was used as electrolyte for all the tests unless otherwise specified. After 20 cyclic voltammetry (CV) cycles, the linear sweep voltammetry curve (LSV) of the activated sample was recorded without iR compensation at a scan rate of 5 mV s$^{-1}$. The recorded potential ($E_{Ag/AgCl}$) was calibrated to the reversible hydrogen electrode (RHE) using the Nernst equation: $E_{RHE} = E_{Ag/Ag/Cl} + 0.0591\ pH + 0.197$. Electrochemical impedance spectroscopy

(EIS) was carried out at the onset potential from 100 kHz to 0.01 Hz and the transfer resistance ($R_{ct}$) values were calculated based on the equivalent circuit. To estimate the electrochemically active surface area (ECSA), CV cycling was performed at different scan rates. For the durability test, the chronopotentiometric measurements were conducted at 50 mA $cm^{-2}$ for 24 h. Overall, water splitting was carried out in an ordinary electrolyzer with bifunctional NiCu/IF as the anodic electrode and cathodic electrode.

## 3. Results and Discussion

### *3.1. Structural Characterization*

The preparation process of the bifunctional self-supported NiCu/IF electrodes is illustrated in Scheme 1. In such a one-step electrosynthesis process, the soluble SCN anode serves as a Ni and Cu precursor. SEM is an effective method for analyzing the microstructure of materials. Figure 1a,b and Figure S1 present the representative SEM images of the as-fabricated NiCu/IF and original IF electrodes. Clearly, pure IF has a smooth surface, while NiCu/IF has a microflowers structure composed of nanometer-thick flakes. Also, it can be seen that the NiCu microflowers which are composed of nanometer-thick flakes assembled on the porous IF substrate to form a typical self-supported NiCu/IF electrode with abundant surface areas and active sites, suggesting great potential applications in water electrolysis. The corresponding EDS elemental mapping images in Figure 1c indicate the homogeneous distribution of Ni, Cu, and O elements on the microflowers catalysts (Fe element originated from the IF substrate). To investigate the phase composition and crystal structure of the prepared electrode, the XRD pattern was collected as shown in Figure S2. The broad diffraction peaks (approximately 35 and 60°) may be due to the formation of an alloy of Cu and Ni [49,50]. In addition, the ultrathin nanosheet structure as shown in Figure 1d, and the thickness is less than 20 nm, and the length and width are between 60 and 120 nm. As shown in the high-resolution TEM (HRTEM) image (Figure 1e), the lattice fringes of around 0.2034 and 0.2087 nm corresponding to (111) planes of Ni and Cu can be observed, and meanwhile no conspicuous diffraction signals are found in the corresponding SAED pattern (inset of Figure 1e).

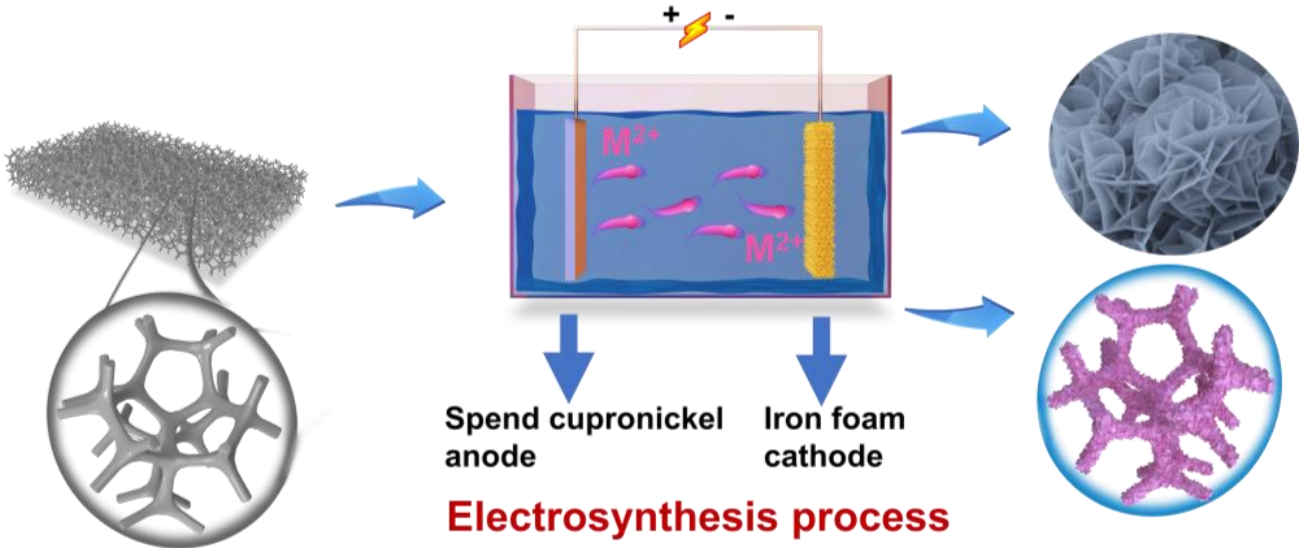


**Scheme 1.** Schematic illustration of the electrosynthesis process for the self-supported nanostructural NiCu/IF electrode.

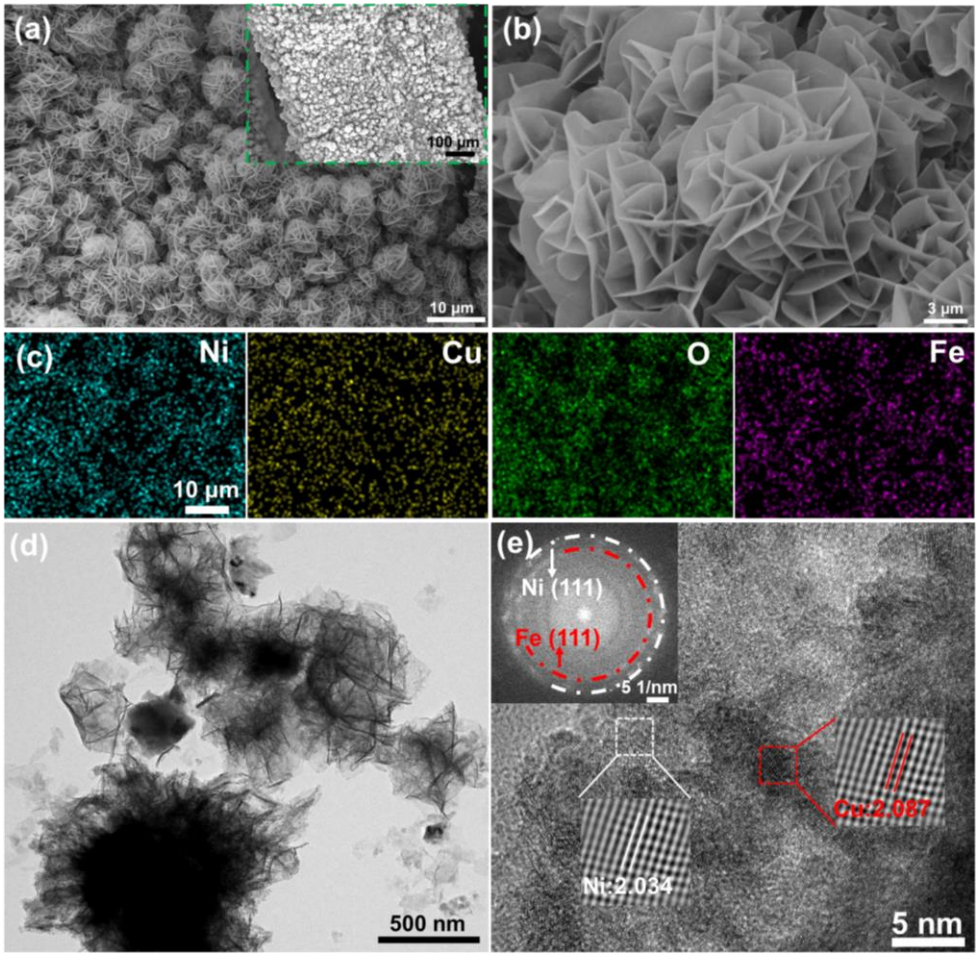


**Figure 1.** (**a**,**b**) SEM images, (**c**) EDS spectrum, (**d**,**e**) TEM images and the SAED pattern of NiCu/IF.

To further clarify the chemical structure and composition of the NiCu/IF electrode, Raman and XPS measurements were also performed. Figure 2a shows the series of Raman demonstrated that the catalyst consists of nickel oxide. Specifically, the Raman shift at 300–600 $cm^{-1}$ is the most complicated, which includes the one-phonon (TO and LO modes). The Raman peak at ~1080 $cm^{-1}$ can be attributed to 2LO modes [51,52]. The XPS can be an effective way to reveal completely elemental compositions and chemical states on the surface of NiCu/IF. The XPS spectra in Figure 2b–d confirms the presence of Ni, Cu, and O. As shown in Figure 2b, the Ni 2p spectrum can be fitted into two spin-orbit peaks, i.e., Ni $2p_{1/2}$ and Ni $2p_{3/2}$ located at 874 and 856 eV with two shakeup satellites. It can reveal that Ni is in the $Ni^{2+}$ oxidation state [53,54]. It is coincident with the Raman pattern results in Figure 2a. The Cu 2p spectrum (Figure 2c) shows the Cu 2p3/2 and Cu 2p1/2 peaks located at 931.8 eV and 951.1 eV, suggesting the existence of Cu [20]. The above results can indicate that SCN anode dissolved into the solution and was then deposited on the IF cathode during the electrolysis process. The O 1s spectrum of NiCu/IF is displayed in Figure 2d. The fitted peak located at 531.5 eV can correspond to surface-adsorbed water and hydroxy species, and the other peaks at around 529.5 eV can be attributed to lattice oxygen in metal oxides [55]. Therefore, from the aforementioned physical characterization, it can be concluded that the microflowers NiCu/IF electrode was successfully fabricated using the SCN anode as a precursor in a two-electrode electrolysis. In addition, SEM, XRD, and XPS were also carried out to the CN/IF electrode, and the results are shown in Figures S3 and S4. Figure S3 shows the electrode has a microstructure similar to NiCu/IF. A subtle difference is that the nanosheets are thicker and form microspheres instead of microflowers after reunion. In Figure S5a, the XRD results display that the CN/IF consists of two phases:

Fe and Cu. Apparently, Fe originated from the IF. Corresponding to this is the XPS result (Figure S3b–d); there are characteristic peaks of nickel oxide, copper oxide and Cu.

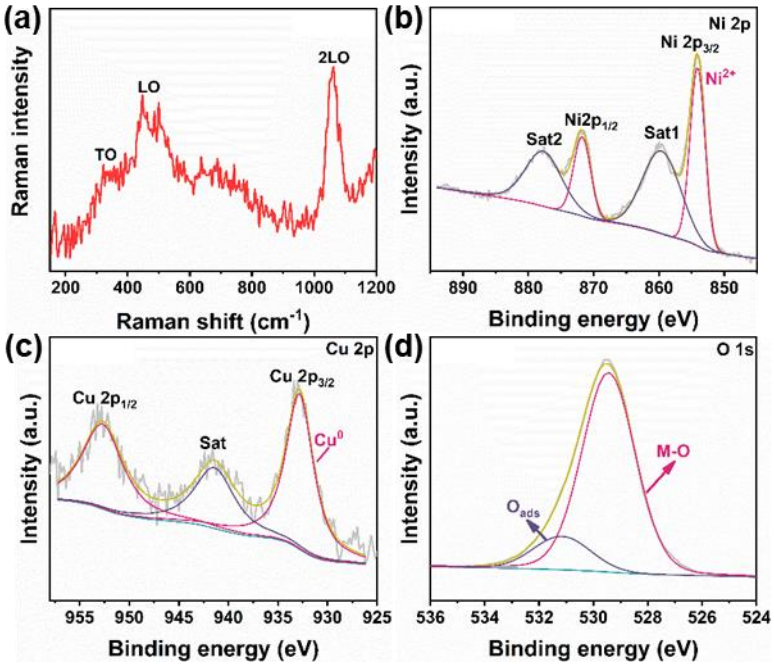


**Figure 2.** (**a**) Raman of NiCu/IF. XPS spectra of (**b**) Ni 2p, (**c**) Cu 2p, and (**d**) O 1s for the self-supported NiCu/IF electrode.

### *3.2. Electrochemical Performance*

Figure 3 shows the electrocatalytic performance of the designed NiCu/IF, CN/IF, pure IF, and commercial catalysts (Pt/C and $RuO_2$) in 1 M KOH solution. To evaluate electrocatalysis activity, the NiCu/IF, CN/IF, pure IF, and commercial precious metal catalyst (Pt/C and $RuO_2$) were appraised. The LSV of NiCu/IF, CN/IF, and IF are presented in Figure 3a. NiCu/IF exhibits a boosted HER activity (overpotential of 96 mV at 10 mA $cm^{-2}$), closing to 20 wt% Pt/C (43 mV), in distinct contrast to CN/IF (259 mV) and bare IF (284 mV), as well as the recently reported bifunctional transition metal electrocatalysts (Table S1). Indeed, a large number of samples were prepared in the process of exploring the best preparation conditions (Figures S5 and S6). To further elucidate the role of the NiCu/IF during the HER process, the Raman analysis was implemented via various voltages from −1.0 to −1.4 vs. Ag/AgCl. As shown in Figure 3b and Figure S7, when no voltage was applied, the Raman spectrum peak exhibits the characteristic peak of nickel oxide. However, with the voltage increase from −1.0 to −1.4 vs. Ag/AgCl, the nickel oxide is gradually transformed into $Ni(OH)_2$, where the Raman peak is located at 450 $cm^{-1}$ and 520 $cm^{-1}$ [56,57]. Moreover, the Tafel curve was employed to investigate the reaction kinetics of the HER. The Tafel slope of NiCu/IF was calculated as 74.8 mV $dec^{-1}$, which is lower than those of CN/IF (191.8 mV $dec^{-1}$), and pure IF (178.1 mV $dec^{-1}$), meaning the rapid kinetics of the HER (Figure 3c). To evaluate the intrinsic activity of these hybrid electrodes, the ECSA was gauged using the double-layer capacitor ($C_{dl}$). The CV curves of the prepared electrocatalysts were measured at various scan rates from 20 to 100 mV $s^{-1}$ (Figure S8a–c). The $C_{dl}$ value of NiCu/IF (13.4 mF $cm^{-2}$) is significantly higher than that of other electrocatalysts, which manifests that NiCu/IF supplies a greater number of electrocatalytic active surfaces for the water splitting reaction. EIS was employed to investigate the underlying mechanism of highly efficient water splitting. The Nyquist plots of NiCu/IF and other electrocatalysts were presented in Figure 3d. Combined with the illustrations, it shows that NiCu/IF possesses the smallest charge transfer resistance, indicating a faster electron transfer and a greater mass transport. The sufficient specific surface area of the NiCu nanosheets and the highly conductive porous pure foamed metallic

iron skeleton boost the exposure of sufficient catalytic active surfaces and the ability to quicken the charge transfer.

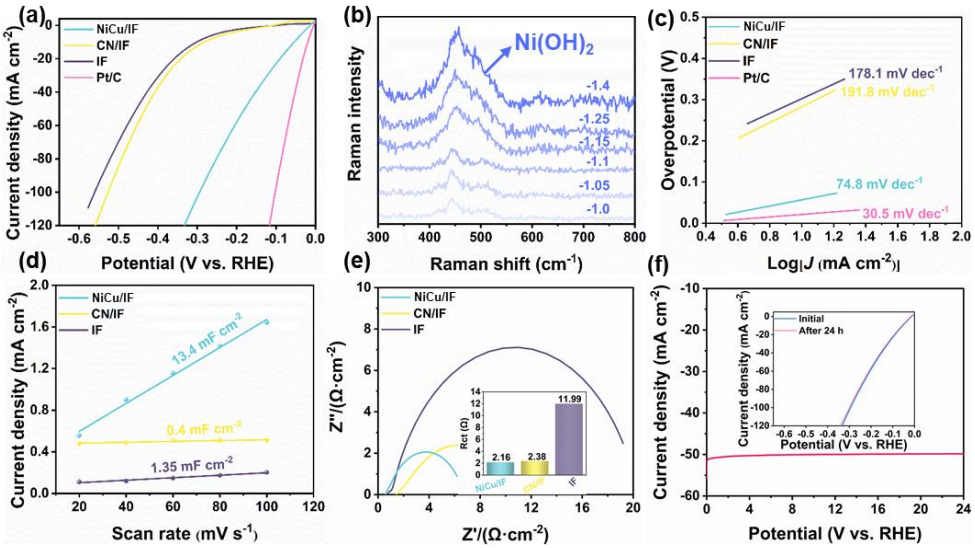


**Figure 3.** (**a**) LSV curves of NiCu/IF, CN/IF, IF, and commercial Pt/C in 1 M KOH. (**b**) The Raman spectroscopy measurements of NiCu/IF in HER electrocatalysis. (**c**) Tafel slopes of NiCu/IF, CN/IF, and IF for the HER. (**d**) ECSA value of electrocatalysts for the HER obtained from the CV test in an alkaline electrolyte. (**e**) EIS and $R_{ct}$ value of electrocatalysts for the HER. (**f**) The galvanostatic assay of NiCu/IF at 50 mA $cm^{-2}$ for the HER; inset: LSV curves of NiCu/IF initial and after 24 h i-t test.

Stability parameters are vital for the electrocatalyst in practical industrialization applications. The durability of NiCu/IF was probed by a long i-t test for over 24 h under the 50 mA $cm^{-2}$ (Figure 3f). LSV curves after 24 h displayed no significant change in activity compared with the initial curve (inset, Figure 3f), exhibiting outstanding long-term stability. After continuous catalysis for over 24 h, no significant fluctuations in their corresponding curves are observed.

Meanwhile, the OER performances of the NiCu/IF, CN/IF and IF were also probed in a 1 M KOH. The NiCu/IF electrode exhibits the best OER performance among the above materials; the overpotentials at $\eta_{10}$ and $\eta_{50}$ are 256 and 345 mV, respectively, lower those of CN/IF (340 and 420 mV) and IF (486 and 558 mV), and close to $RuO_2$ (280 and 345 mV). Especially for pure IF electrodes, to obtain 50 mA $cm^{-2}$ working current density, its overpotential is higher than the NiCu/IF electrode 213 mV. It is evident that the synthesized Ni-Cu microflowers possess outstanding electrocatalytic activity for OER. In addition, according to many other reported non-noble electrocatalyst in electro-catalyzing OER in Table S1, the NiCu/IF can compete with the recently reported bifunctional transition metal electrocatalysts. To further elucidate the catalytic mechanism of the NiCu/IF during the OER process, the Raman technique was implemented via various voltages from 1.1 to 1.6 vs. RHE. As shown in Figure 4b, when no voltage was applied, the Raman spectrum peak exhibits the characteristic peak of nickel oxide. However, with the voltage increase from 1.1 to 1.6 vs. RHE, this nickel oxide is gradually transformed into NiOOH where the Raman peak is located at 470 $cm^{-1}$ and 550 $cm^{-1}$. Previous studies demonstrate that the active NiOOH can efficiently and robustly oxidate water and other small molecules at a relatively low potential [58–60]. Moreover, the corresponding Tafel slope from the anodic scan in Figure 4c, the NiCu/IF also has a smaller value (50.82 mV $dec^{-1}$) than those of CN/IF, IF, and $RuO_2$, suggesting that NiCu/IF possesses a faster OER rate. To evaluate the intrinsic activity of these hybrid electrodes, the ECSA was gauged by the $C_{dl}$. The CV curves of the prepared electrocatalysts were measured at various scan rates from 20 to 100 mV $s^{-1}$ (Figure S9). As seen Figure 4e, the $C_{dl}$ value of NiCu/IF (23.4 mF $cm^{-2}$) is significantly higher than that of other electrocatalysts, which demonstrates that NiCu/IF

supplies a greater number of electrocatalytic active surfaces for the water splitting reaction.

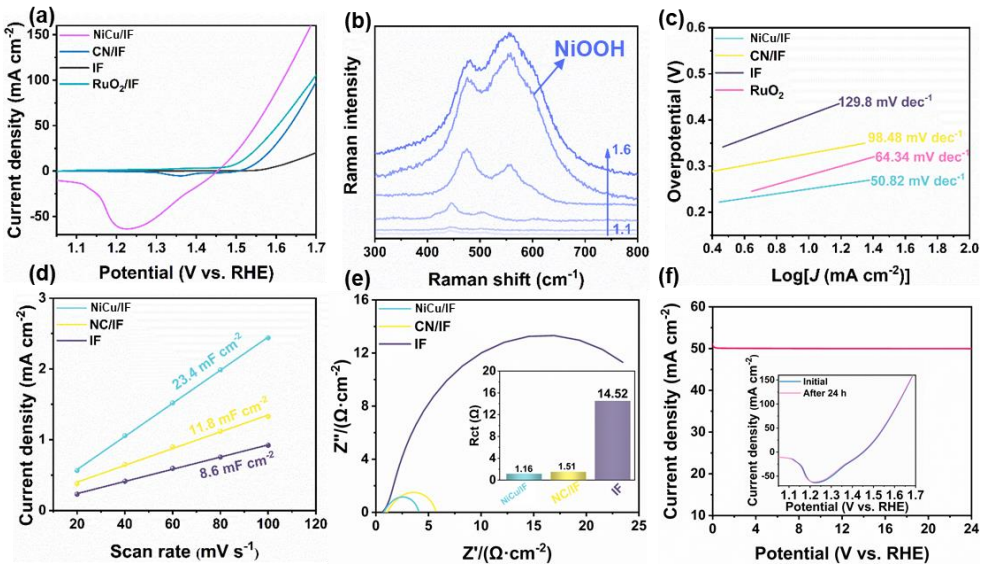


**Figure 4.** (**a**) LSV curves of NiCu/IF, CN/IF and IF, compared with the curve of the commercial Pt/C in an alkaline electrolyte. (**b**) The Raman spectroscopy measurements of NiCu/IF in OER electrocatalysis. (**c**) Tafel slopes of electrocatalysts for the OER were obtained from the LSV curves. (**d**) ECSA value of electrocatalysts for the OER obtained from the CV test in an alkaline electrolyte. (**e**) EIS and $R_{ct}$ value of electrocatalysts for the HER obtained from the CV test in an alkaline electrolyte. (**f**) The galvanostatic assay of NiCu/IF at 50 mA $cm^{-2}$ for the OER; inset: LSV curves of NiCu/IF before and after 24 h i-t test.

The EIS was employed to investigate the highly efficient water splitting activities. The Nyquist plots of NiCu/IF and other electrocatalysts were presented in Figure 4e. Combined with the illustrations, it shows that NiCu/IF possesses the smallest charge transfer resistance, indicating a faster electron transfer and a greater mass transport. The sufficient specific surface area of the NiCu and the highly conductive porous pure foamed metallic iron skeleton boost the exposure of sufficient catalytic active surfaces and the ability to quicken the charge transfer. The durability of the NiCu microflower was carried out at 50 mA $cm^{-2}$ for a duration of over 24 h (Figure 4f). The durability of NiCu/IF was probed by a long i-t test for 24 h under the 50 mA $cm^{-2}$. LSV curves after 24 h displayed no substantial change in activity compared with the initial curve (inset, Figure 4f), exhibiting outstanding long-term stability. After continuous catalysis for over 24 h, no significant fluctuations in their corresponding curves are observed.

Based on the outstanding catalytic performance and excellent stability of the HER and OER, NiCu/IF was adopted as a double electrode for allover water splitting. NiCu/IF demonstrates excellent catalytic activity, with a cell voltage of 1.57 V at 10 mA $cm^{-2}$, which is close to cells of the Pt/C||$RuO_2$ (Figure 5a), as well as the recently reported bifunctional transition metal electrocatalysts (Figure 5c and Table S1). They exhibit superb stability with a constant 50 mA $cm^{-2}$ for HER and OER, just a slight change after the 24 h i-t test (Figure 5b). It suggests the achievement of robust overall water splitting at a low cell voltage. At a given cell voltage of 1.57 V, a very stable current density of NiCu/IF is observed in Figure 5d. Meanwhile, numerous $O_2$ and $H_2$ bubbles evolved on the surface of NiCu nanosheets. In addition, the HER and GOR two-electrode electrolysis system was established and the LSV curse was collected in 1 M KOH and 0.5 M glycerol as the electrolyte in Figure 5e. More impressively, the as-obtained NiCu/IF electrode for HER&GOR demonstrates outstanding performance, with a cell voltage of 1.29 V at 10 mA $cm^{-2}$. These values are much lower than recently reported transitional metal catalyst (Figure 5f and Table S2). In summary, a novel, efficient and low-cost electrocatalyst from SCN has been synthesized by the one-step electrosynthesis method, which is expected

to become an efficient electrode for the electrocatalytic splitting of water and other small organic molecules.

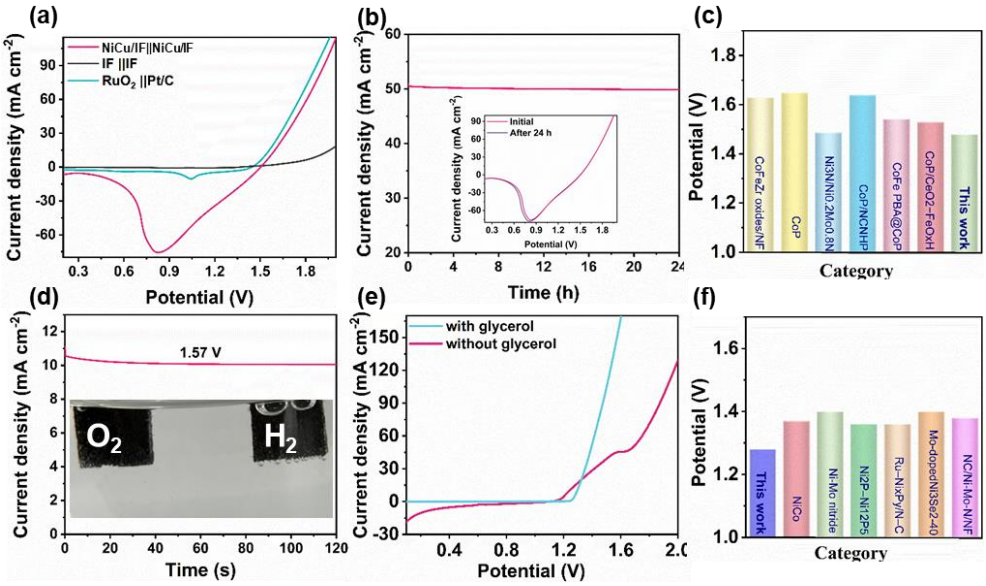


**Figure 5.** (**a**) LSV of NiCu/IF, pure IF, and Pt/C||$RuO_2$ for overall water splitting. (**b**) i-t test and of NiCu/IF at 50 mA $cm^{-2}$ with 24 h; inset: LSV curves of NiCu/IF before and after 24 h i-t test. (**c**) Comparison of the performance of NiCu/IF with those of the recently reported transitional metal bifunctional catalyst in an alkaline electrolyzer. (**d**) The i-t test under 10 mA $cm^{-2}$ with 120 s. (**e**) LSV curves of NiCu/IF for full water splitting in 1 M KOH and 1 M KOH + 0.5 M glycerol. (**f**) Comparison of the performance of NiCu/IF with those of the recently reported transitional metal bifunctional catalyst in 1 M KOH + 0.5 M glycerol.

## 4. Conclusions and Outlook

In summary, novel bifunctional NiCu electrocatalysts were successfully fabricated on the porous IF substrate using one-step electrodeposition utilizing SCN as the soluble anode. The microflowers, which are composed of nanometer-thick flakes, can endow the NiCu electrocatalyst with large specific surface areas and active sites. Highly efficient and stable alkaline HER and OER are achieved over the self-supported NiCu/IF electrodes. Moreover, the assembled NiCu/IF||NiCu/IF full water electrolyzer system also attains a relatively low cell voltage of 1.57 V at 10 mA $cm^{-2}$ with excellent stability. With the introduction of GOR, the electrocatalytic HER performance can be further remarkably enhanced with an extremely low cell voltage of 1.29 V at 10 mA $cm^{-2}$, highlighting an attractive and green route for hydrogen production, coupled with the biomass conversion process. Obviously, the highly efficient novel bifunctional NiCu electrocatalysts have outstanding activity and durability. Nevertheless, to accelerate the large-scale application and rapid development of hydrogen production and waste recovery from green power, the catalytic activity and stability of the catalyst should be enhanced to promote the commercial application of water electrolysis technology, especially decreasing the overpotential at high current density. Moreover, as the SCN has many categories with subtle differences in the composition of elements, it is necessary to ensure the universality of the method and to explore different processes and conditions for different SCN materials. And, more small pollutants (such as hydrazine, formaldehyde, etc.) should be expanded to improve the potential applications of this scheme in environmental remediation and green energy production. On the whole, this work offers a novel electrolysis strategy for the transformation of SCN secondary resources into high-performance NiCu electrocatalysts, which can shed light on the resource recovery and design of superior transition-metal nanomaterials for energy-efficient water electrolysis.

**Supplementary Materials:** The following supporting information can be downloaded at: https://www.mdpi.com/article/10.3390/su151612240/s1, Figure S1. SEM image of IF electrode; Figure S2. XRD pattern of NiCu/IF; Figure S3. SEM images of NC/IF; Figure S4. (a) XRD pattern of NC/IF, (b) XPS Cu 2p, (c) Ni 2p and (d) O 1s of NC/IF; Figure S5. the HER LSV curves of NiCu/IF in different (a) $NiSO_4$ dosage, (b) phosphating time, and (c) phosphating temperature; Figure S6. The OER LSV curves of NiCu/IF in different (a) current, (b) electrodeposition temperature, (c) electrodeposition time, and (d) NiSO4 dosage; Figure S7. The Raman spectroscopy measurements of NiCu/IF in HER electrocatalysis; Figure S8. ECSA of NiCu/IF (a), CV curves of NiCu/IF (b), CN/IF (c), and bare IF (d); Figure S9. ECSA of NiCu/IF (a), CV curves of NiCu/IF (b), CN/IF (c), and bare IF (d). Table S1. Overall water-splitting performances of the representative electrocatalysts in alkaline electrolyte; Table S2. GOR&HER performances of representative electrocatalysts in alkaline electrolyte. Table S3. XRF of spend cupronickel. References [6,8,12,14,16,17,20,36,37,39–42,61–70] are cited in Supplementary Materials.

**Author Contributions:** Z.L.: Material synthesis, data collection, processing and analysis, manuscript writing and revision. Q.W.: manuscript revision, data analysis. Q.K.: Materials characterization and analysis. X.T., S.W. and N.Z.: manuscript review, data analysis. R.X. and L.Y.: Discussion of ideas, review, and editing. All authors have read and agreed to the published version of the manuscript.

**Funding:** This work is supported by the National Natural Science Foundation of China (No. 22262017).

**Institutional Review Board Statement:** This article does not involve research on humans and animals, therefore no ethical declaration is required.

**Informed Consent Statement:** This article does not involve research on humans and animals, therefore no informed consent statement is required.

**Data Availability Statement:** Data available if requested by readers.

**Acknowledgments:** The authors gratefully acknowledge the financial support provided by the National Natural Science Foundation of China (No. 22262017).

**Conflicts of Interest:** The authors declare no conflict of interest.

## References

1. Bodhankar, P.M.; Sarawade, P.B.; Singh, G.; Vinu, A.; Dhawale, D.S. Recent advances in highly active nanostructured NiFe LDH catalyst for electrochemical water splitting. *J. Mater. Chem. A* **2021**, *9*, 3180–3208. [CrossRef]
2. Du, J.; Li, F.; Sun, L. Metal-organic frameworks and their derivatives as electrocatalysts for the oxygen evolution reaction. *Chem. Soc. Rev.* **2021**, *50*, 2663–2695. [CrossRef]
3. Fan, W.; Wang, A.; Wang, L.; Jiang, X.; Xue, Z.; Li, J.; Wang, G. Hollow Carbon Nanopillar Arrays Encapsulated with Pd–Cu Alloy Nanoparticles for the Oxygen Evolution Reaction. *ACS Appl. Mater. Interfaces* **2023**, *15*, 13600–13608. [CrossRef]
4. Li, L.; Wang, P.; Shao, Q.; Huang, X. Metallic nanostructures with low dimensionality for electrochemical water splitting. *Chem. Soc. Rev.* **2020**, *49*, 3072–3106. [CrossRef]
5. Luo, Y.; Zhang, Z.; Chhowalla, M.; Liu, B. Recent Advances in Design of Electrocatalysts for High-Current-Density Water Splitting. *Adv. Mater.* **2022**, *34*, e2108133. [CrossRef]
6. Dong, J.; Wang, Y.; Jiang, Q.; Nan, Z.-A.; Fan, F.R.; Tian, Z.-Q. Charged droplet-driven fast formation of nickel–iron (oxy)hydroxides with rich oxygen defects for boosting overall water splitting. *J. Mater. Chem. A* **2021**, *9*, 20058–20067. [CrossRef]
7. Shah, K.; Dai, R.; Mateen, M.; Hassan, Z.; Zhuang, Z.; Liu, C.; Israr, M.; Cheong, W.C.; Hu, B.; Tu, R.; et al. Cobalt Single Atom Incorporated in Ruthenium Oxide Sphere: A Robust Bifunctional Electrocatalyst for HER and OER. *Angew. Chem. Int. Ed. Engl.* **2022**, *61*, e202114951. [CrossRef]
8. Yin, Z.; Liu, X.; Chen, S.; Xie, H.; Gao, L.; Liu, A.; Ma, T.; Li, Y. Interface engineering of the $MoS_2/NiS_2/CoS_2$ nanotube as a highly efficient bifunctional electrocatalyst for overall water splitting. *Mater. Today Nano* **2021**, *17*, 100156. [CrossRef]
9. Wu, Z.; Zhao, Y.; Wu, H.; Gao, Y.; Chen, Z.; Jin, W.; Wang, J.; Ma, T.; Wang, L. Corrosion Engineering on Iron Foam toward Efficiently Electrocatalytic Overall Water Splitting Powered by Sustainable Energy. *Adv. Funct. Mater.* **2021**, *31*, 2010437. [CrossRef]
10. Wu, X.; Li, J.; Li, Y.; Wen, Z. NiFeP-$MoO_2$ hybrid nanorods on nickel foam as high-activity and high-stability electrode for overall water splitting. *Chem. Eng. J.* **2021**, *409*, 128161. [CrossRef]
11. Shaikh, N.; Mukhopadhyay, I.; Ray, A. Heterointerfaces of nickel sulphides and selenides on Ni-foam as efficient bifunctional electrocatalysts in acidic environments. *J. Mater. Chem. A* **2022**, *10*, 12733–12746. [CrossRef]
12. Singh, T.I.; Rajeshkhanna, G.; Pan, U.N.; Kshetri, T.; Lin, H.; Kim, N.H.; Lee, J.H. Alkaline Water Splitting Enhancement by MOF-Derived Fe-Co-Oxide/Co@NC-mNS Heterostructure: Boosting OER and HER through Defect Engineering and In Situ Oxidation. *Small* **2021**, *17*, 2101312. [CrossRef]

13. Liu, J.; Liu, X.; Shi, H.; Luo, J.; Wang, L.; Liang, J.; Li, S.; Yang, L.-M.; Wang, T.; Huang, Y.; et al. Breaking the scaling relations of oxygen evolution reaction on amorphous NiFeP nanostructures with enhanced activity for overall seawater splitting. *Appl. Catal. B Environ.* **2022**, *302*, 120862. [CrossRef]
14. Sun, Y.; Sun, W.; Chen, L.; Meng, A.; Li, G.; Wang, L.; Huang, J.; Song, A.; Zhang, Z.; Li, Z. Surface reconstruction, doping and vacancy engineering to improve the overall water splitting of CoP nanoarrays. *Nano Res.* **2022**, *16*, 228–238. [CrossRef]
15. Yu, L.; Zhu, Q.; Song, S.; McElhenny, B.; Wang, D.; Wu, C.; Qin, Z.; Bao, J.; Yu, Y.; Chen, S.; et al. Non-noble metal-nitride based electrocatalysts for high-performance alkaline seawater electrolysis. *Nat. Commun.* **2019**, *10*, 5106. [CrossRef]
16. Wang, Y.; Sun, Y.; Yan, F.; Zhu, C.; Gao, P.; Zhang, X.; Chen, Y. Self-supported NiMo-based nanowire arrays as bifunctional electrocatalysts for full water splitting. *J. Mater. Chem. A* **2018**, *6*, 8479–8487. [CrossRef]
17. Rani, B.J.; Sivanantham, A.; Shridharan, T.S.; Runfa, T.; Cho, I.S. Faceted and defect-rich $CuMn_2O_4$ nanoparticles for efficient electrochemical water splitting. *J. Mater. Chem. A* **2022**, *10*, 17710–17720. [CrossRef]
18. Zhao, G.; Yao, Y.; Lu, W.; Liu, G.; Guo, X.; Tricoli, A.; Zhu, Y. Direct Observation of Oxygen Evolution and Surface Restructuring on $Mn_2O_3$ Nanocatalysts Using In Situ and Ex Situ Transmission Electron Microscopy. *Nano Lett.* **2021**, *21*, 7012–7020. [CrossRef]
19. Liu, C.; Han, Y.; Yao, L.; Liang, L.; He, J.; Hao, Q.; Zhang, J.; Li, Y.; Liu, H. Engineering Bimetallic NiFe-Based Hydroxides/Selenides Heterostructure Nanosheet Arrays for Highly-Efficient Oxygen Evolution Reaction. *Small* **2021**, *17*, e2007334. [CrossRef]
20. Su, H.; Jiang, J.; Li, N.; Gao, Y.; Ge, L. NiCu alloys anchored defect-rich NiFe layered double-hydroxides as efficient electrocatalysts for overall water splitting. *Chem. Eng. J.* **2022**, *446*, 137226. [CrossRef]
21. Roy, S.; Bagchi, D.; Dheer, L.; Sarma, S.C.; Rajaji, V.; Narayana, C.; Waghmare, U.V.; Peter, S.C. Mechanistic insights into the promotional effect of Ni substitution in non-noble metal carbides for highly enhanced water splitting. *Appl. Catal. B Environ.* **2021**, *298*, 120560. [CrossRef]
22. Zhou, Z.; Wang, Q.; Yao, H.; Wang, M.; Wu, P.; Wang, H.; Zhang, L.; Guo, L. Rapid Synthesis of C60-MoC Nanocomposites by Molten Salt Electrolysis for Hydrogen Evolution. *J. Electrochem. Soc.* **2023**, *170*, acb853. [CrossRef]
23. Ganesan, P.; Sivanantham, A.; Shanmugam, S. Nanostructured Nickel-Cobalt-Titanium Alloy Grown on Titanium Substrate as Efficient Electrocatalyst for Alkaline Water Electrolysis. *ACS Appl. Mater. Interfaces* **2017**, *9*, 12416–12426. [CrossRef]
24. Gao, M.Y.; Yang, C.; Zhang, Q.B.; Zeng, J.R.; Li, X.T.; Hua, Y.X.; Xu, C.Y.; Dong, P. Facile electrochemical preparation of self-supported porous Ni–Mo alloy microsphere films as efficient bifunctional electrocatalysts for water splitting. *J. Mater. Chem. A* **2017**, *5*, 5797–5805. [CrossRef]
25. Gebreslase, G.A.; Martínez-Huerta, M.V.; Lázaro, M.J. Recent progress on bimetallic NiCo and CoFe based electrocatalysts for alkaline oxygen evolution reaction: A review. *J. Energy Chem.* **2022**, *67*, 101–137. [CrossRef]
26. Wang, J.; Xin, S.; Xiao, Y.; Zhang, Z.; Li, Z.; Zhang, W.; Li, C.; Bao, R.; Peng, J.; Yi, J.; et al. Manipulating the Water Dissociation Electrocatalytic Sites of Bimetallic Nickel-Based Alloys for Highly Efficient Alkaline Hydrogen Evolution. *Angew. Chem. Int. Ed. Engl.* **2022**, *61*, e202202518. [CrossRef]
27. Subbaraman, R.; Tripkovic, D.; Chang, K.C.; Strmcnik, D.; Paulikas, A.P.; Hirunsit, P.; Chan, M.; Greeley, J.; Stamenkovic, V.; Markovic, N.M. Trends in activity for the water electrolyser reactions on 3d M(Ni,Co,Fe,Mn) hydr(oxy)oxide catalysts. *Nat. Mater.* **2012**, *11*, 550–557. [CrossRef]
28. Dai, L.; Chen, Z.N.; Li, L.; Yin, P.; Liu, Z.; Zhang, H. Ultrathin Ni(0)-Embedded $Ni(OH)_2$ Heterostructured Nanosheets with Enhanced Electrochemical Overall Water Splitting. *Adv. Mater.* **2020**, *32*, e1906915. [CrossRef]
29. Molla, C.F.; Gonfa, B.A.; Sabir, F.K.; Gicha, B.B.; Nwaji, N.; Tufa, L.T.; Lee, J. Ni-based ultrathin nanostructures for overall electrochemical water splitting. *Mater. Chem. Front.* **2023**, *7*, 194–215. [CrossRef]
30. Lu, X.; Xie, S.; Yang, H.; Tong, Y.; Ji, H. Photoelectrochemical hydrogen production from biomass derivatives and water. *Chem. Soc. Rev.* **2014**, *43*, 7581–7593. [CrossRef]
31. Zhu, W.; Yue, Z.; Zhang, W.; Hu, N.; Luo, Z.; Ren, M.; Xu, Z.; Wei, Z.; Suo, Y.; Wang, J. Wet-chemistry topotactic synthesis of bimetallic iron–nickel sulfide nanoarrays: An advanced and versatile catalyst for energy efficient overall water and urea electrolysis. *J. Mater. Chem. A* **2018**, *6*, 4346–4353. [CrossRef]
32. Adhikari, S.; Kwon, Y.; Kim, D.-H. Three-dimensional core–shell structured $NiCo_2O_4$@CoS/Ni-Foam electrocatalyst for oxygen evolution reaction and electrocatalytic oxidation of urea. *Chem. Eng. J.* **2020**, *402*, 126192. [CrossRef]
33. Fan, L.; Ji, Y.; Wang, G.; Chen, J.; Chen, K.; Liu, X.; Wen, Z. High Entropy Alloy Electrocatalytic Electrode toward Alkaline Glycerol Valorization Coupling with Acidic Hydrogen Production. *J. Am. Chem. Soc.* **2022**, *144*, 7224–7235. [CrossRef]
34. Li, S.; Ma, P.; Gao, C.; Liu, L.; Wang, X.; Shakouri, M.; Chernikov, R.; Wang, K.; Liu, D.; Ma, R.; et al. Reconstruction-induced NiCu-based catalysts towards paired electrochemical refining. *Energy Environ. Sci.* **2022**, *15*, 3004–3014. [CrossRef]
35. Wang, Q.; Ma, X.; Wu, P.; Li, B.; Zhang, L.; Shi, J. CoNiFe-LDHs decorated $Ta_3N_5$ nanotube array photoanode for remarkably enhanced photoelectrochemical glycerol conversion coupled with hydrogen generation. *Nano Energy* **2021**, *89*, 106326. [CrossRef]
36. Liu, X.; Fang, Z.; Teng, X.; Niu, Y.; Gong, S.; Chen, W.; Meyer, T.J.; Chen, Z. Paired formate and $H_2$ productions via efficient bifunctional Ni-Mo nitride nanowire electrocatalysts. *J. Energy Chem.* **2022**, *72*, 432–441. [CrossRef]
37. Morales, D.M.; Jambrec, D.; Kazakova, M.A.; Braun, M.; Sikdar, N.; Koul, A.; Brix, A.C.; Seisel, S.; Andronescu, C.; Schuhmann, W. Electrocatalytic Conversion of Glycerol to Oxalate on Ni Oxide Nanoparticles-Modified Oxidized Multiwalled Carbon Nanotubes. *ACS Catal.* **2022**, *12*, 982–992. [CrossRef]

38. Pei, Y.; Pi, Z.; Zhong, H.; Cheng, J.; Jin, F. Glycerol oxidation-assisted electrochemical $CO_2$ reduction for the dual production of formate. *J. Mater. Chem. A* **2022**, *10*, 1309–1319. [CrossRef]
39. Pu, H.; Dong, K.; Zhang, T.; Dai, H.; Wang, Y.; Deng, Y. Regulation of the shell thickness and shell components in PtCu/PdCu core–shell tripods for ethylene glycol and glycerol oxidation reactions. *J. Mater. Chem. A* **2022**, *10*, 10614–10624. [CrossRef]
40. Wang, G.; Chen, J.; Li, K.; Huang, J.; Huang, Y.; Liu, Y.; Hu, X.; Zhao, B.; Yi, L.; Jones, T.W.; et al. Cost-effective and durable electrocatalysts for Co-electrolysis of $CO_2$ conversion and glycerol upgrading. *Nano Energy* **2022**, *92*, 106751. [CrossRef]
41. Xu, Y.; Liu, T.; Shi, K.; Yu, H.; Deng, K.; Wang, X.; Wang, Z.; Wang, L.; Wang, H. Ru-doping induced lattice strain in hetero-phase $Ni_2P$–$Ni_{12}P_5$ arrays enables simultaneous efficient energy-saving hydrogen generation and formate electrosynthesis. *J. Mater. Chem. A* **2022**, *10*, 20365–20374. [CrossRef]
42. Yu, H.; Wang, W.; Mao, Q.; Deng, K.; Wang, Z.; Xu, Y.; Li, X.; Wang, H.; Wang, L. Pt single atom captured by oxygen vacancy-rich NiCo layered double hydroxides for coupling hydrogen evolution with selective oxidation of glycerol to formate. *Appl. Catal. B Environ.* **2023**, *330*, 122617. [CrossRef]
43. Hao, J.; Zhuang, Z.; Cao, K.; Gao, G.; Wang, C.; Lai, F.; Lu, S.; Ma, P.; Dong, W.; Liu, T.; et al. Unraveling the electronegativity-dominated intermediate adsorption on high-entropy alloy electrocatalysts. *Nat. Commun.* **2022**, *13*, 2662. [CrossRef]
44. Wang, Y.; Xue, Y.; Zhang, C. Enhanced anodic dissolution of cupronickel alloy scraps by electro-generated reactive oxygen species in acid media. *J. Alloys Compd.* **2019**, *806*, 106–112. [CrossRef]
45. Zhao, Y.; Peng, L.; Xie, H.; Zhang, W.; Huang, S.; Yang, Z.; Li, Z.; Mi, X. Enhancing the erosion–corrosion resistance of cupronickel alloy through grain boundary engineering. *Corros. Sci.* **2023**, *219*, 111228. [CrossRef]
46. Arab, N.; Fotouhi, L.; Salis, A. Electrosynthesised CdS@ZnS quantum dots decorated multi walled carbon nanotubes for analysis of propranolol in biological fluids and pharmaceutical samples. *Microchem. J.* **2021**, *168*, 106453. [CrossRef]
47. Ballarin, B.; Berrettoni, M.; Carpani, I.; Scavetta, E.; Tonelli, D. Electrodes modified with an electrosynthesised Ni/Al hydrotalcite as amperometric sensors in flow systems. *Anal. Chim. Acta* **2005**, *538*, 219–224. [CrossRef]
48. Wu, L.; Yu, L.; McElhenny, B.; Xing, X.; Luo, D.; Zhang, F.; Bao, J.; Chen, S.; Ren, Z. Rational design of core-shell-structured CoP @FeOOH for efficient seawater electrolysis. *Appl. Catal. B Environ.* **2021**, *294*, 120256. [CrossRef]
49. Serre, C.; Yaakoubi, N.; Martínez, S.; Pérez-Rodríguez, A.; Morante, J.R.; Esteve, J.; Montserrat, J. Electrochemical deposition of Cu and Ni/Cu multilayers in Si Microsystem Technologies. *Sens. Actuators A Phys.* **2005**, *123–124*, 633–639. [CrossRef]
50. Yao, H.; Xie, L.; Cheng, Y.; Duan, J.; Chen, Y.; Lyu, S.; Sun, Y.; Liu, J. Tuning the coercivity of Cu/Ni multilayer nanowire arrays by tailoring multiple parameters. *Mater. Des.* **2017**, *123*, 165–173. [CrossRef]
51. Deshpande, M.P.; Patel, K.N.; Gujarati, V.P.; Patel, K.; Chaki, S.H. Structural, Thermal and Optical Properties of Nickel Oxide (NiO) Nanoparticles Synthesized by Chemical Precipitation Method. *Adv. Mater. Res.* **2016**, *1141*, 65–71. [CrossRef]
52. Song, M.-T.; Zhang, Y.; Huang, W.-J.; Hou, H.-Y.; Chen, X.-B. Enhancement of two-magnon scattering in annealed nickel oxide studied by Raman spectroscopy. *Acta Phys. Sin.* **2021**, *70*, 167201. [CrossRef]
53. López, M.C.; Ortiz, G.F.; Lavela, P.; Alcántara, R.; Tirado, J.L. Improved Energy Storage Solution Based on Hybrid Oxide Materials. *ACS Sustain. Chem. Eng.* **2012**, *1*, 46–56. [CrossRef]
54. Lu, X.; Zhao, C. Electrodeposition of hierarchically structured three-dimensional nickel-iron electrodes for efficient oxygen evolution at high current densities. *Nat. Commun.* **2015**, *6*, 6616. [CrossRef]
55. Ye, K.; Li, K.; Lu, Y.; Guo, Z.; Ni, N.; Liu, H.; Huang, Y.; Ji, H.; Wang, P. An overview of advanced methods for the characterization of oxygen vacancies in materials. *TrAC Trends Anal. Chem.* **2019**, *116*, 102–108. [CrossRef]
56. Wu, Y.J.; Yang, J.; Tu, T.X.; Li, W.Q.; Zhang, P.F.; Zhou, Y.; Li, J.F.; Li, J.T.; Sun, S.G. Evolution of Cationic Vacancy Defects: A Motif for Surface Restructuration of OER Precatalyst. *Angew. Chem. Int. Ed. Engl.* **2021**, *60*, 26829–26836. [CrossRef]
57. Faid, A.Y.; Barnett, A.O.; Seland, F.; Sunde, S. Ni/NiO nanosheets for alkaline hydrogen evolution reaction: In situ electrochemical-Raman study. *Electrochim. Acta* **2020**, *361*, 137040. [CrossRef]
58. Zheng, L.; Zhao, Y.; Xu, P.; Lv, Z.; Shi, X.; Zheng, H. Biomass upgrading coupled with $H_2$ production via a nonprecious and versatile Cu-doped nickel nanotube electrocatalyst. *J. Mater. Chem. A* **2022**, *10*, 10181–10191. [CrossRef]
59. Huang, Y.; Wang, J.-J.; Zou, Y.; Jiang, L.-W.; Liu, X.-L.; Jiang, W.-J.; Liu, H.; Hu, J.-S. Selective Se doping of $NiFe_2O_4$ on an active NiOOH scaffold for efficient and robust water oxidation. *Chin. J. Catal.* **2021**, *42*, 1395–1403. [CrossRef]
60. Wang, H.; Guan, A.; Zhang, J.; Mi, Y.; Li, S.; Yuan, T.; Jing, C.; Zhang, L.; Zheng, G. Copper-doped nickel oxyhydroxide for efficient electrocatalytic ethanol oxidation. *Chin. J. Catal.* **2022**, *43*, 1478–1484. [CrossRef]
61. Deng, Y.; Cao, Y.; Xia, Y.; Xi, X.; Wang, Y.; Jiang, W.; Yang, D.; Dong, A.; Li, T. Self-Templated Synthesis of CoFeP@C Cage-In-Cage Superlattices for Enhanced Electrocatalytic Water Splitting. *Adv. Energy Mater.* **2022**, *12*, 43. [CrossRef]
62. Zhao, X.; Zheng, X.; Lu, Q.; Li, Y.; Xiao, F.; Tang, B.; Wang, S.; Yu, D.Y.W.; Rogach, A.L. Electrocatalytic enhancement mechanism of cobalt single atoms anchored on different MXene substrates in oxygen and hydrogen evolution reactions. *EcoMat* **2022**, *5*, 12293. [CrossRef]
63. Gautam, J.; Liu, Y.; Gu, J.; Ma, Z.; Zha, J.; Dahal, B.; Zhang, L.N.; Chishti, A.N.; Ni, L.; Diao, G.; et al. Fabrication of Polyoxometalate Anchored Zinc Cobalt Sulfide Nanowires as a Remarkable Bifunctional Electrocatalyst for Overall Water Splitting. *Adv. Funct. Mater.* **2021**, *31*, 46. [CrossRef]
64. Guo, Y.; Tang, J.; Henzie, J.; Jiang, B.; Xia, W.; Chen, T.; Bando, Y.; Kang, Y.M.; Hossain, M.S.A.; Sugahara, Y.; et al. Mesoporous Iron-doped $MoS_2$/$CoMo_2S_4$ Heterostructures through Organic-Metal Cooperative Interactions on Spherical Micelles for Electrochemical Water Splitting. *ACS Nano* **2020**, *14*, 4141–4152.

65. Huang, L.; Chen, D.; Luo, G.; Lu, Y.R.; Chen, C.; Zou, Y.; Dong, C.L.; Li, Y.; Wang, S. Zirconium-Regulation-Induced Bifunctionality in 3D Cobalt-Iron Oxide Nanosheets for Overall Water Splitting. *Adv. Mater.* **2019**, *31*, e1901439. [CrossRef]
66. Ji, L.; Wang, J.; Teng, X.; Meyer, T.J.; Chen, Z. CoP Nanoframes as Bifunctional Electrocatalysts for Efficient Overall Water Splitting. *ACS Catal.* **2019**, *10*, 412–419. [CrossRef]
67. Li, R.-Q.; Wan, X.-Y.; Chen, B.-L.; Cao, R.-Y.; Ji, Q.-H.; Deng, J.; Qu, K.-G.; Wang, X.-B.; Zhu, Y.-C. Hierarchical $Ni_3N/Ni_{0.2}Mo_{0.8}N$ heterostructure nanorods arrays as efficient electrocatalysts for overall water and urea electrolysis. *Chem. Eng. J.* **2021**, *409*, 128240. [CrossRef]
68. Pan, Y.; Sun, K.; Liu, S.; Cao, X.; Wu, K.; Cheong, W.C.; Chen, Z.; Wang, Y.; Li, Y.; Liu, Y.; et al. Core-Shell ZIF-8@ZIF-67-Derived CoP Nanoparticle-Embedded N-Doped Carbon Nanotube Hollow Polyhedron for Efficient Overall Water Splitting. *J. Am. Chem. Soc.* **2018**, *140*, 2610–2618. [CrossRef]
69. Quan, L.; Li, S.; Zhao, Z.; Liu, J.; Ran, Y.; Cui, J.; Lin, W.; Yu, X.; Wang, L.; Zhang, Y.; et al. Hierarchically Assembling CoFe Prussian Blue Analogue Nanocubes on CoP Nanosheets as Highly Efficient Electrocatalysts for Overall Water Splitting. *Small Methods* **2021**, *5*, e2100125. [CrossRef]
70. Yang, L.; Liu, R.; Jiao, L. Electronic Redistribution: Construction and Modulation of Interface Engineering on CoP for Enhancing Overall Water Splitting. *Adv. Funct. Mater.* **2020**, *30*, 1909618.